Environ Earth Sci (2011) 64:2223–2228
DOI 10.1007/s12665-011-1050-8

ORIGINAL ARTICLE

Pore-scale removal mechanisms of residual light non-aqueous phase liquids in porous media

Helian Li · Jiajun Chen · Jian Yang

Received: 4 January 2010 / Accepted: 25 March 2011 / Published online: 8 April 2011
© Springer-Verlag 2011

Abstract Glass-etched micromodel and visualization technology were used to research the removal mechanisms of residual light non-aqueous phase liquids (LNAPLs) droplets at pore scale. In this research, *n*-hexadecane was selected as the LNAPL model substance. During the injection of de-ionized water into the pore channel, residual *n*-hexadecane droplet was removed quickly at first, then gradually became slow and finally remained nearly invariable; the droplet size after a definite time depends on its initial value. The relationship between total volume of residual *n*-hexadecane and time can be described by a logarithmic equation: $V = V_0 - 0.0152\ln t + 0.0360$ ($0 < t < 9{,}420$, $R^2 = 0.9621$). Based on percolation theory, the relationship between fluid percolation velocity in pores and time was determined through the analysis of residual *n*-hexadecane droplet size and the flowing characteristics of injected fluid. Gaussian model was used to fit the cumulated dissolved *n*-hexadecane, the correlation coefficient $R^2 = 0.97269$. The removal process of *n*-hexadecane in network model experiment is similar to that of the sand column flushing experiment, which indicates that the mass transfer micro-mechanism of network model experiment could be used to interpret the results of column flushing experiment.

Keywords LNAPLs · Network model · Porous media · Pore · Removal mechanism

H. Li · J. Chen (✉)
State Key Laboratory of Water Environment Simulation, School of Environment, Beijing Normal University, Beijing 100875, China
e-mail: jeffchen@bnu.edu.cn

H. Li
School of Resources and Environment, University of Jinan, Jinan 250022, China

J. Yang
Institute of Nuclear and New Technology, Tsinghua University, Beijing 100084, China

J. Yang
Beijing Drainage Group Company Limited, Beijing 100038, China

Introduction

Non-aqueous phase liquids (NAPLs) contamination will change the soil physicochemical characteristics, posing severe threat to human and animals (Ting et al. 1999; Vasudevan and Rajaram 2001). Spillage and leakage accidents during petroleum production and processing, storage and shipping are the main sources of NAPLs contamination (Vasudevan and Rajaram 2001). Due to interaction of capillary and interfacial forces between the subsurface and contaminant, NAPLs can become trapped in the soil pores in the form of non-continuous globules (Duffield et al. 2003), which are difficult to remove. Researchers have done some jobs from different scales to investigate the migration and displacement rule of NAPLs in soils (Cooper et al. 1998; Reddi et al. 1998; Lee et al. 2002; Taylor et al. 2004; Wood et al. 2005; Putzlocher et al. 2006). Researches at Mega- and macro-scale can get general laws of NAPLs migration. Studies at micro-scale would enhance understanding of the micro-mechanisms of NAPLs migration in porous media. Network model experiment is an effective method that can be used to investigate NAPLs migration at micro scale.

Network model research could be dated back to 1950s, when the concept of network model was first put forward

by Fatt (1956a, 1956b, 1956c). In petroleum area, network model has been used to research the size distribution of residual oil droplets (Egbogah and Dawe 1980), the immiscible displacement of gas-oil (Campbell and On 1985), trapping of NAPLs in pore and throat (Wardlaw 1982), permeability and dispersivity (Corapcioglu et al. 1997; Corapcioglu and Fedirchuk 1999; Theodoropoulou et al. 2003), the relationship between relative permeability and capillary pressure (Theodoropoulou et al. 2005), and so on. In the recent years, with the increasing concern for NAPLs contamination, network model was used to visualize the removal process of residual NAPLs in soil and aquifer. For example, Jeong et al. (2000) studied the mass transfer processes during NAPL remediation; Jia et al. (1999) investigated the removal mechanisms of trichloroethylene by surfactant foam; Jeong and Corapcioglu (2003) researched the factors influencing the removal of NAPL by surfactant foam flooding; Sharmin et al. (2006) researched the effect of surfactant partitioning on the dissolution kinetics of residual perchloroethylene (PCE) by Triton X-100 solution; Sahloul et al. (2002) investigated the pore-scale removal mechanism and mass transfer rates of residual NAPL. To our knowledge, a little work has been done on the quantitative relationships between the residual/dissolved LNAPLs and percolation time of injected fluid at pore scale.

This paper aims to the following goals: (1) observing the removal processes of residual LNAPLs at pore scale, (2) establishing quantitative relationships between the residual/dissolved LNAPLs and percolation time of injected fluid, which would be useful to the design of remediation projects.

Materials and methods

Chemical materials

The chemical reagents used in this research are analytical grade *n*-hexadecane (Tianjin Chemical Research Institute, China) and Sudan IV (Tianjin Chemical Research Institute, China). Sudan IV was added to the *n*-hexadecane to enhance its visibility. De-ionized water was produced by Beijing Jiangchuan water treatment technology Co. Ltd. Other materials include: 10 mL beakers used to contain *n*-hexadecane, 100 mL Erlenmeyer flasks used to collect waste liquids.

Experimental set-up

Figure 1 shows the experimental setup used in this research. It is composed of SMZ-168 stereomicroscope (Motic China Group Co. Ltd, China); Motic Images Advanced 3.2 image acquisition and processing system (Motic China Group Co. Ltd, China); TJ-3A syringe pump (Lange Constant Flow Pump Co. Ltd, Baoding, China); glass micromodel (Xinyi Instrument Co. Ltd, Yixing, China); silica gel pipes; glass injector (Shanghai Zhenge Medical Injector Co. Ltd, China); computer. The micromodel was put in the view field of the stereomicroscope. Motic Images Advanced 3.2 image acquisition and processing system was installed on the computer. Video camera was installed on the stereomicroscope.

Digital pattern of the micromodel pore network, and inlet and outlet channels, were designed using AutoCAD software. A glass plate was selected to be refinished and polished before the pattern was etched on it. The etched glass plate was washed in an ultrasonic cleaner. Another glass plate was put onto the etched one and they were hot bonded together. Dyed de-ionized water was injected to check up the connectivity of the glass model. There were six pores in the micromodel, with coordination number of four. The mean pore and throat radius are 0.244 and 0.091 mm, respectively, which are the statistical pore and throat radius values of media composed of coarse sand with particle size of 0.5–1 mm. The depths of pores and throats are 0.182 mm.

Methods

Connection and debugging

The apparatus were connected according to Fig. 1. Every part should be adjusted to make the apparatus work in harmony. Adjustment includes the following aspects: (1) Stereomicroscope: appropriate microscope stage and size of object lens were chosen according to the object size and observing scope. Halogen bulb or ring lamp should be selected according to demand for light. Ring lamp was used in this research for its excellent performance such as low heat emission, soft and natural light, no color distortion, and

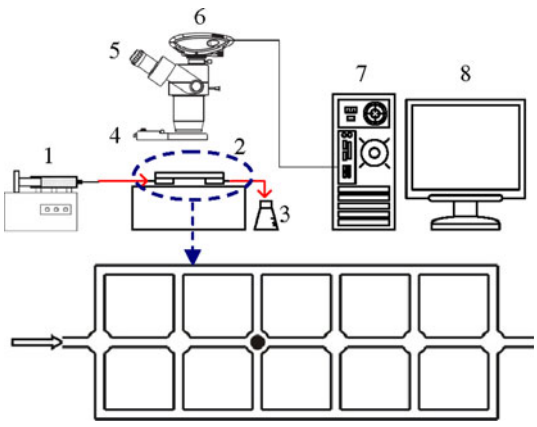

Fig. 1 Experiment set-up: *1* syringe pump, *2* network models, *3* outflow collection, *4* ring lamp, *5* stereomicroscope, *6* moticam device, *7* PC, *8* monitor

efficiency in easing the eyestrain. (2) Computer: data acquisition and analysis system was connected with stereomicroscope through data lines. The data acquisition and analysis software was set up. (3) Syringe pump: proper injector was fixed onto the syringe pump. (4) Micromodel: two silica gel pipes were connected to the micromodel. One at the inlet was used to connect the micromodel and the syringe pump, the other at the outlet was used to discharge the waste liquids into the waste collector.

Parameter optimizing

In order to acquire clear images, parameters of experimental apparatus were optimized. Main operations were as follows: (1) the object distance of stereomicroscope was adjusted and kept unchanged in the whole experimental process; (2) adjusting exposal parameters, setting up image size, collection and store mode through the software; (3) choosing the right injector model and manipulate mode of syringe pump. Manipulate modes include infuse, withdraw, infuse first then withdraw, withdraw first then infuse. Infuse mode was used in the experiment; setting parameters of injected fluid volume, infuse/withdraw time, distribution and interval times; (4) adjusting the position of the network model in the vision field.

Calibration

The stereomicroscope was calibrated with calibration slides (1,500,600 μm). The true size of each pixel stands for should be established according to the image of calibration slides. The injector size (internal diameter/flow rate) was calibrated through the calibration mode. The flow rate was calibrated through comparing the measured and the set fluid flow rate.

Images acquisition and processing

At different experimental stages, images were collected and processed by Motic Images Advanced 3.2 (Fig. 2). The images were processed through the following steps: (1) choosing the image region needed to process; (2) color segmentation and noise removal; (3) choosing target object, calculating its area, percentage, perimeter, roundness, radius of its equivalent area circle, and some other parameters.

Results and discussion

Volume change of residual *n*-hexadecane

The micromodel was initially saturated with *n*-hexadecane at a constant volumetric flow rate of 0.167 mL/h, followed by injection of de-ionized water at the same flow rate to establish conditions of trapped *n*-hexadecane ganglia. The research started at the time when *n*-hexadecane ganglia were formed (Fig. 3a). Water was continuously injected and the dissolution process of individual ganglia was monitored. Figure 3 is snapshots of the dissolution evolution of single *n*-hexadecane ganglion. Figure 4 is the projected area change of residual *n*-hexadecane ganglion during de-ionized water injection. Define pore numbers as 1–6 from left to right on the micromodel. According to Figs. 3 and 4, it is evident that the area of *n*-hexadecane decreased remarkably at the interval of 0–3,420 s. At the time of 0 s, there was residual *n*-hexadecane in all the six pores. The drops in pore one and six were smaller than the others. This is because pore one and pore six were directly connected to the inlet and outlet of the micromodel, the fluid pressures in pore one and pore six were bigger than that in other pores. In the process of displacing NAPL with water to form residual NAPL droplet, all the influx flowed

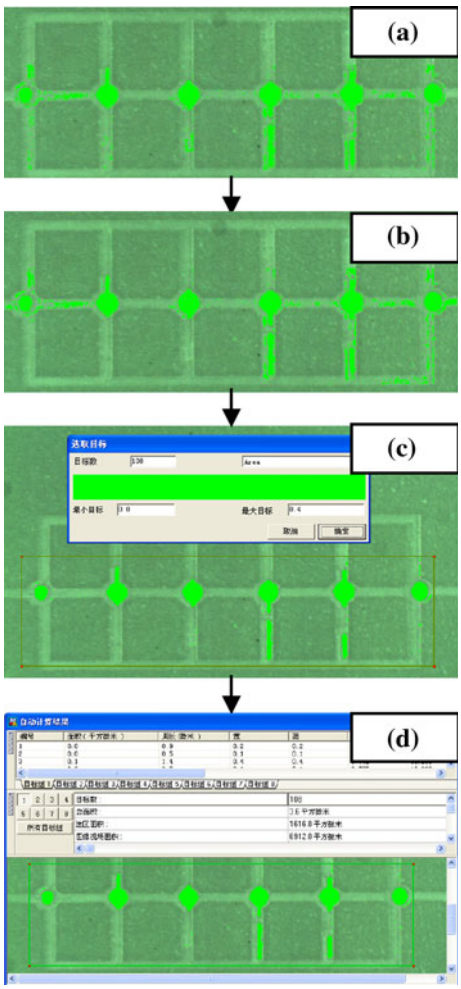

Fig. 2 Image data processing (**a**) electing range and color dividing, (**b**) removing offending points, (**c**) choosing calculation objects, (**d**) calculating objects

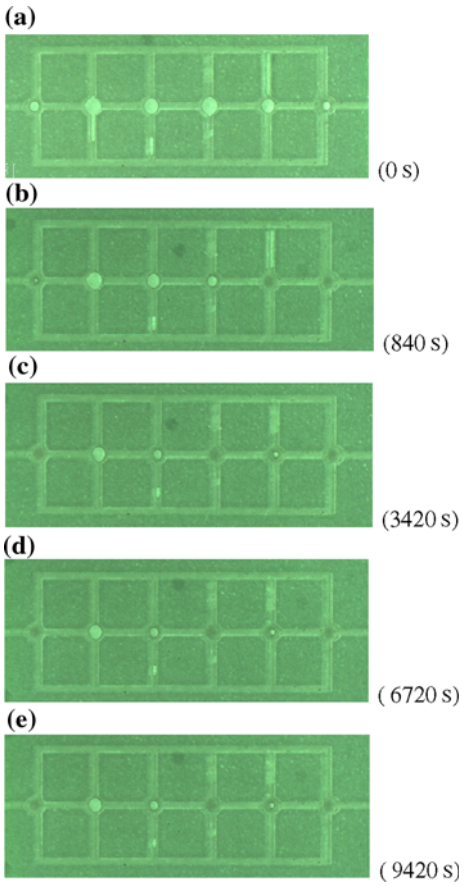

Fig. 3 Snapshots of the dissolution evolution of single *n*-hexadecane droplet

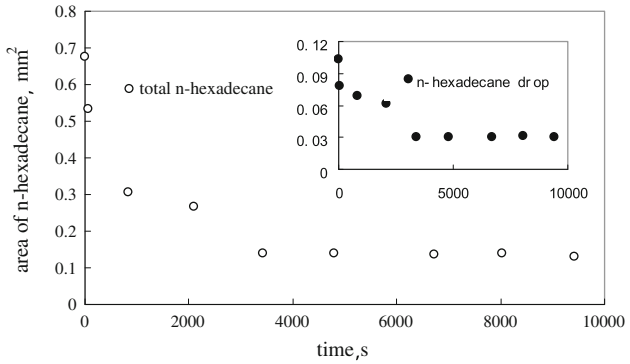

Fig. 4 Area changing of *n*-hexadecane during de-ionized water injected

through pore one and pore six, so the drops of the pore one and six would be smaller than the others. For the same reason, the displacement and dissolution of NAPL drops in pore one and pore six would be faster than the others. At the time of 840 s, there was no residual *n*-hexadecane in the fifth and the sixth pore. At the time of 3,420 s, there was no residual *n*-hexadecane in the first, the fourth and the sixth pore, while there was *n*-hexadecane again in the fifth pore. The experiment was repeated several times, although there were some differences in the drop size for a given pore in all the experiments, this phenomenon appeared every time. This can be explained as follows: at the initial time, the hexadecane was displaced by water, then, the *n*-hexadecane in other pores and throats was displaced into this pore again. After 3,420 s, the area of residual *n*-hexadecane remained nearly invariable. There are two possible conditions. One is that the changes of the residual *n*-hexadecane were too small to discern, the other is that there was no influx to the pore, the *n*-hexadecane would also remain constant. The droplet size after a definite time depends on its initial value. The relationship between total residual *n*-hexadecane volume and time can be described by a logarithmic equation: $V = V_0 - 0.0152\ln t + 0.0360$ ($0 < t < 9{,}420$, $R^2 = 0.9621$), where V_0 is the initial volume of residual *n*-hexadecane. The *n*-hexadecane volume equals to the product of the projected area and the pore depth.

Residual NAPL droplet dissolution characteristics

To analyze the relationship between the removal of single NAPL droplet and the total NAPLs in the same flow channel, the residual droplet in the third pore was chosen to do analysis. The evolution of the total NAPLs projected areas in the micromodel was compared with that of a single NAPL droplet (Fig. 4). It can be seen that the dissolution rule of single droplet is the same as that of the total NAPLs, indicating that the dissolution of total residual NAPLs can be reflected by single residual droplet in the same flow channel. Analyzing the change of single residual *n*-hexadecane, it can be found that the *n*-hexadecane droplet diminished rapidly at first, then removal became slower, finally, the residual *n*-hexadecane remained nearly invariable. The changing process was closely related to the flow rate of injected fluid in the pores.

Figure 5 is a conceptual model of pore-scale mass transfer from a single trapped NAPL ganglion given by Sahloul et al. (2002). Water flows around the trapped NAPL droplet, mass transfer by convection and diffusion occurs in the space between the pore wall and the NAPL/water interface. As time goes on, organic solute is transported by convection and diffusion away from the NAPL/water interface, the trapped NAPL ganglion becomes smaller and smaller, and the distance between the pore wall and the NAPL/water interface increases, which can be described as follows:

$$S = R - r \tag{1}$$

where S is the distance between the pore wall and the NAPL/water interface, R is the pore radius, r is the radius of NAPL droplet which changes with time

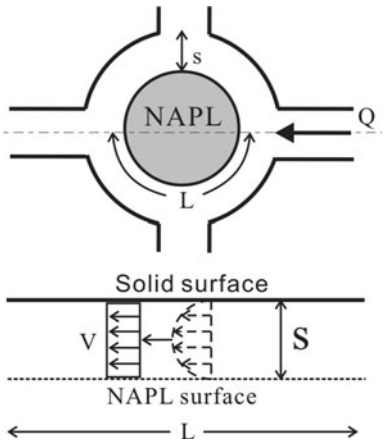

Fig. 5 Mass transfer model of NAPL in pores (after Sahloul et al. 2002)

$$r = \sqrt{A/\pi} \tag{2}$$

where, A is the projected area of NAPL droplet. In this study, the value of A in pore three can be fitted with t as follows:

$$A = A_0 - 0.011\ln t + 0.0271 (R^2 = 0.7932) \tag{3}$$

where A_0 is the initial projected area of NAPL droplet.

Water velocity, u can be simply calculated by the following equation:

$$u = \frac{Q}{2S \cdot D} \tag{4}$$

where Q is the flow rate of injected fluid, D is the depth of pore channel. Then the flow velocity as a function of time can be written as:

$$u = \frac{Q}{2(R - \sqrt{(A_0 - 0.011 \ln t + 0.0271)/\pi}) \cdot D} \tag{5}$$

As time goes on, the NAPL ganglia decreases in size, the water flow velocity decreases. When injection flux is constant, the concentration gradient between water and NAPL decreases. Furthermore, the interface area between water and NAPL decreases too. The mass transfer becomes slower and slower. The projected area of residual NAPL droplet decreases rapidly then tends to remain a steady state. This phenomenon is similar to the result of soil column flushing experiment where dissolution of residual NAPL is a rate-limited process and present a tailing effect (Boving and Brusseau 2000; Bradford et al. 2003). It appeared that the macro phenomenon in column flushing can be explained by the microcosmic mass transfer mechanism in the pore-scale network model.

To obtain the changing rule of *n*-hexadecane dissolution in a single pore, Gaussian model was used to fit the cumulated dissolved *n*-hexadecane quantity normalized by micromodel volume as a function of time. The Gaussian model is as follows:

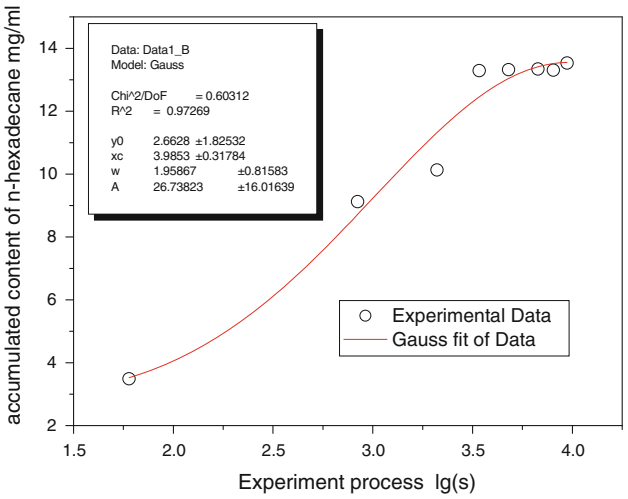

Fig. 6 Gaussian model fitting of the cumulated dissolved *n*-hexadecane quantity per unit volume as a function of time

$$y = y_0 + \frac{A}{w \cdot \sqrt{\frac{\pi}{2}}} e^{-\frac{2(x-x_0)^2}{w^2}} \tag{6}$$

where y is the cumulated dissolved *n*-hexadecane quantity normalized by micromodel volume; x is time (s). Model (6) involves four fitting parameters; the meaning of each parameter is as follows: y_0 is baseline offset, A is total area under the curve from the baseline, x_0 is center of the peak, w is 2σ approximately 0.849 the width of the peak at half height.

Figure 6 is the Gaussian model fitting result, the correlation coefficient $R^2 = 0.97269$, which means that Gaussian model could describe the changing characteristics of cumulated dissolved *n*-hexadecane quantity normalized by micromodel volume.

Conclusions

Based on pore network model, residual LNAPLs droplet removal experiment was done in this paper, and some conclusions can be drawn:

(1) Displaced by water, residual *n*-hexadecane droplet was removed quickly at first, then gradually became slow and finally remained nearly invariable, the droplet size after a definite time depends on its initial value. The changing rule of single residual *n*-hexadecane droplet is as the same to the total *n*-hexadecane volume in the same flow channel. The relationship between total residual *n*-hexadecane volume and time can be described by a logarithmic equation: $V = V_0 - 0.0152\ln t + 0.0360$ ($0 < t < 9{,}420$, $R^2 = 0.9621$).

(2) According to percolation theory, the flow rate of injected fluid in pores as a function of time can be obtained through analysis of residual *n*-hexadecane droplet projected area and the flow characteristics of injected fluid.
(3) The dissolution of residual NAPL in column flushing can be explained by the microcosmic mass transfer mechanism in the pore-scale network model.
(4) Gaussian model can be used to fit the changing of cumulated dissolved *n*-hexadecane quantity per unit volume as a function of time ($R^2 = 0.97269$).

Acknowledgments This study was financially supported by the National Natural Science Foundation of China (40772148).

References

Boving TB, Brusseau ML (2000) Solubilization and removal of residual trichloroethene from porous media: comparison of several solubilization agents. J Contam Hydrol 42:51–67

Bradford SA, Rathfelder KM, Lang J, Abriola LM (2003) Entrapment and dissolution of DNAPLs in heterogeneous porous media. J Contam Hydrol 67:133–157

Campbell BT, On FM (1985) Flow visualization for CO2/crude-oil displacement. SPE 25:665–678

Cooper GS, Peralta RC, Kaluarachchi JJ (1998) Optimizing separate phase light hydrocarbon recovery from contaminated unconfined aquifers. Adv Water Resour 21:339–350

Corapcioglu MY, Fedirchuk P (1999) Glass bead micromodel study of solute transport. J Contam Hydrol 36:209–230

Corapcioglu MY, Chowdhury S, Roosevelt SE (1997) Micromodel visualization and quantification of solute transport in porous media. Water Resour Res 33:2547–2558

Duffield AR, Ramamurthy RS, Campanelli JR (2003) Surfactant enhanced mobilization of mineral oil within porous media. Water Air Soil Pollut 143:111–122

Egbogah EO, Dawe RA (1980) Microvisual studies of size distribution of oil droplets in porous media. B Can Petrol Geol 28:200–203

Fatt I (1956a) The network model of porous media I. Capillary characteristics. Pet. Trans. AIME 207:144–159

Fatt I (1956b) The network model of porous media II. Dynamic properties of a single size tube network. Pet Trans AIME 207:160–163

Fatt I (1956c) The network model of porous media III. Dynamic properties of networks with tube radius distribution. Pet Trans AIME 207:164–181

Jeong SW, Corapcioglu MY (2003) A micromodel analysis of factors influencing NAPL removal by surfactant foam flooding. J Contam Hydrol 60:77–96

Jeong SW, Corapcioglu MY, Roosevelt SE (2000) Micromodel study of surfactant foam remediation of residual trichloroethylene. Environ Sci Technol 34:3456–3461

Jia C, Shing K, Yortsos YC (1999) Visualization and simulation of non-aqueous phase liquids solubilization in pore networks. J Contam Hydrol 35:363–387

Lee D, Cody RD, Kim DJ, Choi S (2002) Effect of soil texture on surfactant-based remediation of hydrophobic organic-contaminated soil. Environ Int 27:681–688

Putzlocher R, Kueper BH, Reynolds DA (2006) Relative velocities of DNAPL and aqueous phase plume migration. J Contam Hydrol 88:321–336

Reddi LN, Menon S, Pant A (1998) Pore-scale investigations on vibratory mobilization of LNAPL ganglia. J Hazard Mater 62:211–230

Sahloul NA, Ioannidis MA, Chatzis I (2002) Dissolution of residual non-aqueous phase liquids in porous media: pore-scale mechanisms and mass transfer rates. Adv Water Resour 25:33–49

Sharmin R, Ioannidis MA, Legge RL (2006) Effect of nonionic surfactant partitioning on the dissolution kinetics of residual perchloroethylene in a model porous medium. J Contam Hydrol 82:145–164

Taylor TP, Rathfelder KM, Pennell KD, Abriola LM (2004) Effects of ethanol addition on micellar solubilization and plume migration during surfactant enhanced recovery of tetrachloroethene. J Contam Hydrol 69:73–99

Theodoropoulou MA, Karoutsos V, Kaspiris C, Tsakiroglou CD (2003) A new visualization technique for the study of solute dispersion in model porous media. J Contam Hydrol 274:176–197

Theodoropoulou MA, Sygouni V, Karoutsos V, Tsakiroglou CD (2005) Relative permeability and capillary pressure functions of porous media as related to the displacement growth pattern. Int J Multiphas Flow 31:1155–1180

Ting YP, Hu HL, Tan HM (1999) Bioremediation of petroleum hydrocarbons in soil microcosms. Res Environ Biotechnol 2:197–218

Vasudevan N, Rajaram P (2001) Bioremediation of oil sludge-contaminated soil. Environ Int 26:409–411

Wardlaw N (1982) The effects of geometry, wettability, viscosity and interfacial tension on trapping in single pore-throat pairs. J Can Petrol Tech 21:21–27

Wood AL, Enfield CG, Espinoza FP, Annable M, Brooks MC, Rao PSC, Sabatini D, Knox R (2005) Design of aquifer remediation systems: (2) Estimating site-specific performance and benefits of partial source removal. J Contam Hydrol 81:148–166